EPJ Web of Conferences **356**, 01033 (2026) https://doi.org/10.1051/epjconf/202635601033
ICC 2025

Transition metal-doped glasses for radiation shielding applications

Chandrasekhar Maalegoundla[a*], *Kotha Aruna Kumari*[a], *Rajesham* Siddoju[b], R.*Umamaheswara Singh*[c]

[a]Matrusri Engineering College, Saidabad, Hyderabad, Telangana, India-500059
[b]Geethanjali college of Engineering and Technology, Cheeryal, Keesara, Medchal, Telangana, India-501301
[c]Hyderabad Institute of Technology and Management, Hyderabad, Telangana, India-501401

Abstract. To examine the impact of systematic compositional changes on the radiation shielding capabilities of manganese dioxide (MnO_2) doped boro-bismuth glasses-two distinct glass series were synthesized: one with a lead fluoride (PbF_2) base and the other with a calcium fluoride (CaF_2) base, where the concentration of Al_2O_3 was progressively increased from 3 to 15 mol% at the expense of the (PbF_2) and (CaF_2). The non-crystalline structure of the glasses was confirmed by XRD analysis. The density and radiation-shielding parameters, including the mass attenuation coefficient (MAC,μm) and effective atomic number (Zeff), were measured using the Stimulating software Phy-X/PSD. For the PbF_2-based series, density decreased from 4.49 to 4.13 g/cm³, MAC dropped from 88.64 cm^2/gm to 75.37 cm^2/gm, and Z_{eff} decreased from 77.99 to 75.85. For the CaF_2-based series, density decreased from 3.73 to 3.35 g/cm³, MAC: 58.746 to 56.279 cm²/g and Z_{eff} rose from 66.74 to 67.69. Lead-based glasses provide the best radiation shielding, according to the data, whereas calcium-based glasses have tunable characteristics and are safer and more environmentally friendly. These materials can be used in medical imaging, radiotherapy facilities, nuclear power plants, aerospace applications, and portable radiation protection since adding Al_2O_3 greatly increases their strength and radiation shielding capacity.

1 Introduction

Glass systems are frequently employed in various applications due to their adaptable qualities, which include strength, transparency, and design flexibility. Glasses are used to protect patients and medical personnel from radiation exposure in various settings, including linear accelerators, CT scanners, and X-ray rooms. Additionally, radiation shielding glasses are employed at waste storage facilities, nuclear power plants, and research institutions to safeguard the environment and employees from radiation risks [1]. By absorbing or deflecting various rays and particles, these radiation shielding glasses lower the total radiation dosage that a person receives. Attenuation, which describes the progressive

* Corresponding author: sekharfgx@gmail.com

decrease in radiation intensity as it travels through a material, is the fundamental idea underlying shielding. Shielding materials are carefully chosen based on effectiveness and feasibility in settings where radiation safety is crucial. Lead, lead-free substitutes, and lead-based composites are the most often utilised materials.[2]. The development of non-toxic, lead-free shielding materials has also been made possible by technological advancements. Lead is substituted with other attenuating elements, including antimony (Sb), tungsten (W), and tin (Sn). They provide comparable protection against scattered radiation. One of the many advantages of lead-free shielding is that it is non-toxic and recyclable. Additionally, lead-free shielding materials may be lighter, making them more comfortable for staff to wear throughout extended operations. From the standpoint of neutron control, boron-rich glasses are appealing due to the high cross-section of boron compared to other elements. The capacity of borate glasses to absorb charged radiation and provide gamma shielding is enhanced when heavy ions are added to their matrix. Bi_2O_3 has better radiation shielding qualities, while the lower atomic number Al and O atoms improved the glass system's capacity to interact with fast neutrons [3,4]. In this study, glasses were prepared using the composition (30-x) PbF_2-xAl_2O_3-$10Bi_2O_3$-$59B_2O_3$-$1MnO_2$ and (30-x) CaF_2-xAl_2O_3-$10Bi_2O_3$-$59B_2O_3$-$1MnO_2$ (where x=3,6,9,12,15) and studied radiation shielding parameters.

2. Materials and Methods

2.1 Preparation of glass samples

Two series of manganese dioxide (MnO_2) doped boro-bismuth glasses in every five samples, with the composition (30-x) PbF_2-xAl_2O_3-$10Bi_2O_3$-$59B_2O_3$-$1MnO_2$ and (30-x) CaF_2-xAl_2O_3-$10Bi_2O_3$-$59B_2O_3$-$1MnO_2$ (where x=3,6,9,12,15) were prepared using the melt and quench method. High-purity (99.9%) chemical powders from Aldrich Sigma were weighed according to their molecular percentages using an electronic balance. The mixture was thoroughly ground using a mortar and pestle, transferred to a platinum crucible, and melted in an electric furnace at 1050°C. The resulting melt was rapidly quenched by pouring it onto a steel plate heated to 200°C and pressing it with a second steel plate. The formed glass samples were subsequently annealed for 24 hours. The glass composition, including codes and density values, is presented in **Table 1.**

Table 1: Composition and Density of Glass Samples

Glass code	Composition	Density ρ (cc^{-1})	Glass code	Composition	Density ρ (cc^{-1})
PbMn-1	$27PbF_2$-$3Al_2O_3$ -$10Bi_2O_3$ -$59B_2O_3$ -$1MnO_2$	4.49	**CaMn-1**	$27CaF_2$-$3Al_2O_3$ -$10Bi_2O_3$ -$59B_2O_3$ -$1Mno_2$	3.732
PbMn-2	$24PbF_2$-$6Al_2O_3$ -$10Bi_2O_3$ -$59B_2O_3$ -$1Mno_2$	4.385	**CaMn-2**	$24CaF_2$-$6Al_2O_3$ -$10Bi_2O_3$ -$59B_2O_3$ -$1Mno_2$	3.549
PbMn-3	$21PbF_2$-$9Al_2O_3$ -$10Bi_2O_3$ -$59B_2O_3$ -$1Mno_2$	4.28	**CaMn-3**	$21CaF_2$-$9Al_2O_3$ -$10Bi_2O_3$ -$59B_2O_3$ -$1Mno_2$	3.392
PbMn-4	$18PbF_2$-$12Al_2O_3$ -$10Bi_2O_3$ -$59B_2O_3$ -$1Mno_2$	4.16	**CaMn-4**	$18CaF_2$-$12Al_2O_3$ -$10Bi_2O_3$ -$59B_2O_3$ -$1Mno_2$	3.355
PbMn-5	$15PbF_2$-$15Al_2O_3$ -$10Bi_2O_3$ $_{PbMn}$-$59B_2O_3$ -$1Mno_2$	4.13	**CaMn-5**	$15CaF_2$-$15Al_2O_3$ -$10Bi_2O_3$ -$59B_2O_3$ -$1Mno_2$	3.345

2.2 Theoretical Calculation of Radiation Shielding Parameters

The radiation shielding parameters for the synthesised glass samples were calculated using the **Phy-X/PSD** software code [5]. The parameters determined for gamma-ray energies between 0.015 and 15 MeV include the linear attenuation coefficient (LAC, μ), mass attenuation coefficient (MAC, μ_m), half-value layer (HVL), and effective atomic number (Z_{eff}).

The theoretical foundation for these calculations is provided by the Beer-Lambert law, which describes the attenuation of a photon beam through a material. The law is expressed as:

$$I = I_o e^{-\mu t} \quad (1)$$

where I_o and I are the incident and transmitted radiation intensities, respectively, μ is the linear attenuation coefficient (cm^{-1}), and 't' is the material thickness (cm). The LAC can be derived directly from this relationship:

$$LAC(\mu) = -\frac{ln(\frac{I}{I_0})}{t} \quad (2)$$

The mass attenuation coefficient (MAC, cm^2/g) is defined as the LAC normalised by the material density (ρ):

$$\text{MAC } (\mu_m) = \frac{LAC(\mu)}{\rho} \quad (3)$$

For composite materials like glass, the MAC is calculated using the mixture rule, which sums the contributions from each constituent element

$$MAC = \sum_i w_i MAC_i \quad (4)$$

where w_i is the weight fraction of the I^{th} element.

Key practical shielding parameter, the half-value layer (HVL), represents the material thickness required to reduce the radiation intensity to half and one-tenth of its initial value, respectively. It is calculated as:

$$\text{HVL} = \frac{\ln 2}{\text{LAC}} \quad (5)$$

Finally, the effective atomic number (Z_{eff}) was computed to characterise the overall stopping power of the multi-element glass. It is determined using the formula:

$$\text{Zeff} = \frac{\sum_i f_i A_i MAC_i}{\sum_j f_j \frac{A_j}{Z_j} MAC_j} \quad (6)$$

where for each element, 'f' is the molar fraction, A is the atomic mass, and Z is the atomic number.

3. Results and Discussion

3.1. XRD

In the recorded XRD patterns of PbMn and CaMn samples, no sharp peaks were observed, indicating the amorphous nature of all the glass samples. XRD Patterns are shown in **Fig. 1.**

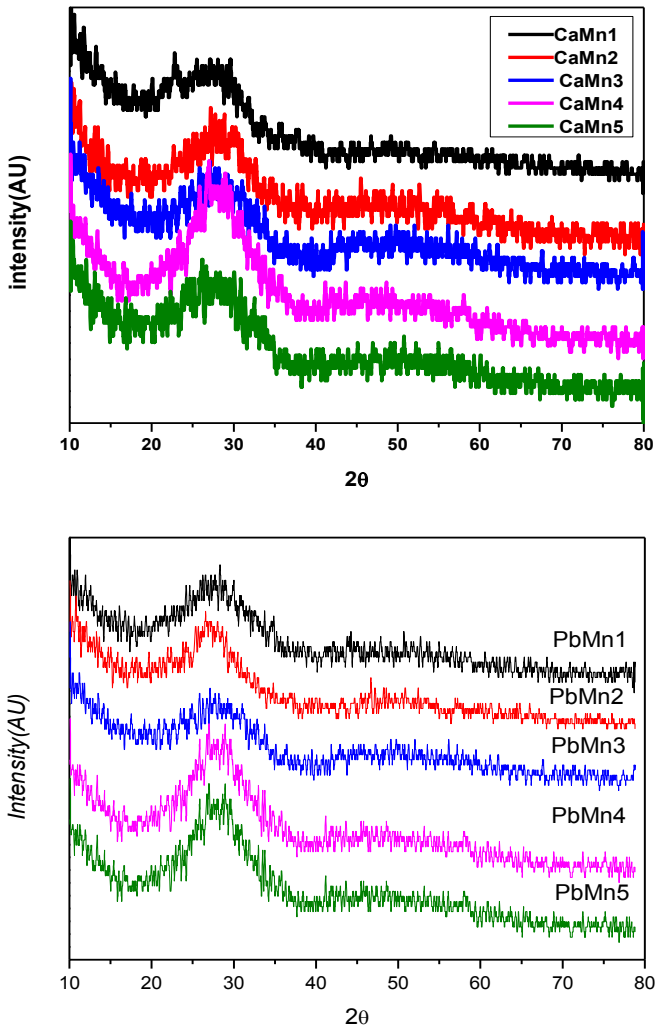

Fig. 1. XRD patterns of PbMn and CaM

3.2. Mass attenuation coefficient (MAC)

The radiation shielding characteristics of multi-element glasses whose densities, chemical formulae, and codes are as seen in **Table 1**. As photon energy rises, MAC falls as depicted in **Figure 2**. This is because the photoelectric effect predominates, and MAC is high at low energy. In both samples, MAC drops from PbMn-1 to PbMn-5 as 88.64 cm^2/gm to 75.37 cm^2/gm and for CaMn-1 to CaMn-5, as 58.746 cm^2/gm to 56.279 cm^2/gm.MAC values are tabulated in **Table 2**. It is due to Compton scattering that takes place at higher energy. MAC of CaMn is significantly lower than the PbMn system. Compared to Pb (Z=82), Ca has a far lower atomic number (Z=20). As a result, it has a much lower photon absorption capability. Although Bi_2O_3 still plays a role, it is insufficient to make up for the reduced Ca. Increase in Al_2O_3, compensating for PbF_2/CaF_2 marginally MAC is decreased [6]. Although the maximum MAC is smaller, Ca-based glasses follow a similar pattern to Pb-based ones. A faster decline is observed at lower energies, while a slow trend is seen at 0.04–0.05 MeV.

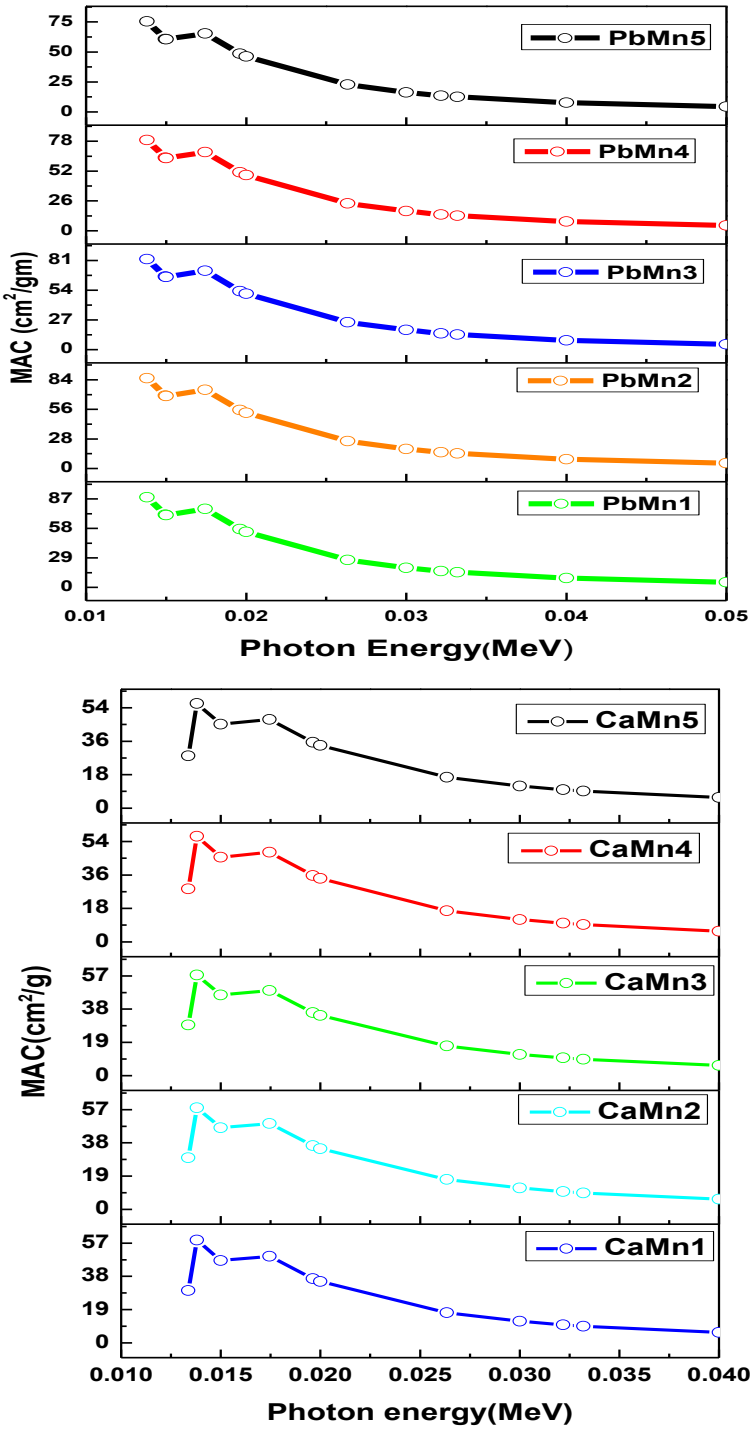

Fig, 2. MAC of PbMn and CaMn

Table 2: MAC Values of PbMn and CaMn Samples

PbMn						CaMn				
	MAC									
Energy (MeV)	PbMn-1	PbMn-2	PbMn-3	PbMn-4	PbMn-5	CaMn-1	CaMn-2	CaMn-3	CaMn-4	CaMn-5
0.013	88.640	85.598	82.381	78.973	75.357	58.746	58.117	57.497	56.884	56.279
0.015	71.511	69.054	66.455	63.703	60.782	47.083	46.581	46.086	45.597	45.114
0.017	77.243	74.523	71.645	68.597	65.363	49.513	49.067	48.626	48.191	47.762
0.019	57.362	55.340	53.201	50.936	48.532	36.712	36.385	36.063	35.744	35.429
0.02	54.733	52.803	50.763	48.601	46.307	35.021	34.710	34.403	34.100	33.800
0.026	26.890	25.944	24.943	23.883	22.758	17.190	17.041	16.894	16.750	16.607
0.03	19.261	18.585	17.869	17.112	16.308	12.314	12.209	12.106	12.004	11.903
0.034	14.805	14.287	13.738	13.157	12.540	9.471	9.391	9.313	9.235	9.159
0.04	9.158	8.839	8.502	8.145	7.766	5.872	5.824	5.776	5.730	5.683
0.05	5.155	4.978	4.790	4.592	4.381	3.324	3.298	3.272	3.247	3.222
0.06	3.240	3.130	3.015	2.892	2.762	2.108	2.092	2.076	2.061	2.046
0.08	1.589	1.538	1.484	1.427	1.367	1.060	1.052	1.045	1.038	1.031
0.1	3.545	3.422	3.291	3.153	3.007	2.234	2.220	2.207	2.193	2.180
0.15	1.316	1.273	1.228	1.180	1.129	0.859	0.855	0.850	0.845	0.840
0.2	0.674	0.654	0.632	0.610	0.586	0.461	0.459	0.456	0.454	0.452
0.3	0.293	0.286	0.279	0.271	0.263	0.221	0.220	0.219	0.218	0.218
0.347	0.227	0.222	0.217	0.212	0.207	0.178	0.177	0.177	0.176	0.176
0.4	0.181	0.178	0.175	0.171	0.167	0.148	0.147	0.147	0.147	0.146
0.5	0.133	0.132	0.130	0.128	0.126	0.115	0.115	0.115	0.115	0.114
0.6	0.108	0.107	0.106	0.105	0.103	0.097	0.097	0.097	0.097	0.097
0.662	0.098	0.097	0.096	0.095	0.094	0.089	0.089	0.089	0.089	0.089
0.8	0.082	0.081	0.081	0.080	0.080	0.077	0.077	0.077	0.077	0.077
1	0.068	0.068	0.068	0.067	0.067	0.066	0.066	0.066	0.066	0.066
1.17	0.060	0.060	0.060	0.060	0.060	0.059	0.059	0.059	0.059	0.059
1.33	0.055	0.055	0.055	0.055	0.055	0.055	0.055	0.055	0.055	0.055
1.5	0.052	0.052	0.052	0.052	0.052	0.052	0.052	0.052	0.052	0.052
2	0.045	0.045	0.045	0.045	0.045	0.045	0.045	0.045	0.045	0.045
2.51	0.042	0.042	0.042	0.041	0.041	0.041	0.041	0.041	0.041	0.041
3	0.040	0.040	0.039	0.039	0.039	0.038	0.038	0.038	0.038	0.038
4	0.038	0.037	0.037	0.037	0.036	0.035	0.035	0.035	0.035	0.035
5	0.037	0.037	0.036	0.036	0.035	0.033	0.033	0.033	0.033	0.033
10	0.039	0.038	0.037	0.037	0.036	0.032	0.032	0.032	0.032	0.032
15	0.042	0.041	0.040	0.039	0.038	0.034	0.033	0.033	0.033	0.033

3.3 Linear attenuation coefficient (LAC)

The linear attenuation coefficient (LAC) for PbMn and CaMn glass systems varies with photon energy, as seen in **Figure 3**. Due to the photoelectric effect's dominance, where

$\mu \propto Z^{4-5}/E^3$. A significant reduction in LAC is seen at low energies between 0.01 and 0.02 MeV, which is followed by a slow fall in the Compton scattering area that is in the higher energy region (≥ 0.05 MeV) [7,1]. Because high-Z Pb and Bi ions are present, PbMn glasses have far higher LAC values than CaMn glasses throughout the whole energy range. For both systems, increasing the Al_2O_3 concentration results in a systematic decrease in LAC; the impact is more noticeable in glasses containing lead. As x increases, Al_2O_3, LAC decrease. For the PbMn series from PbMn-1 to PbMn-5 decrease as 398.48 cm^{-1} to 314.29$cm^{-1,}$ and in the case of the CaMn series from CaMn-1 to CaMn-5 decrease as 219.18 cm^{-1} to 188.03cm^{-1} at 0.0138 MeV.

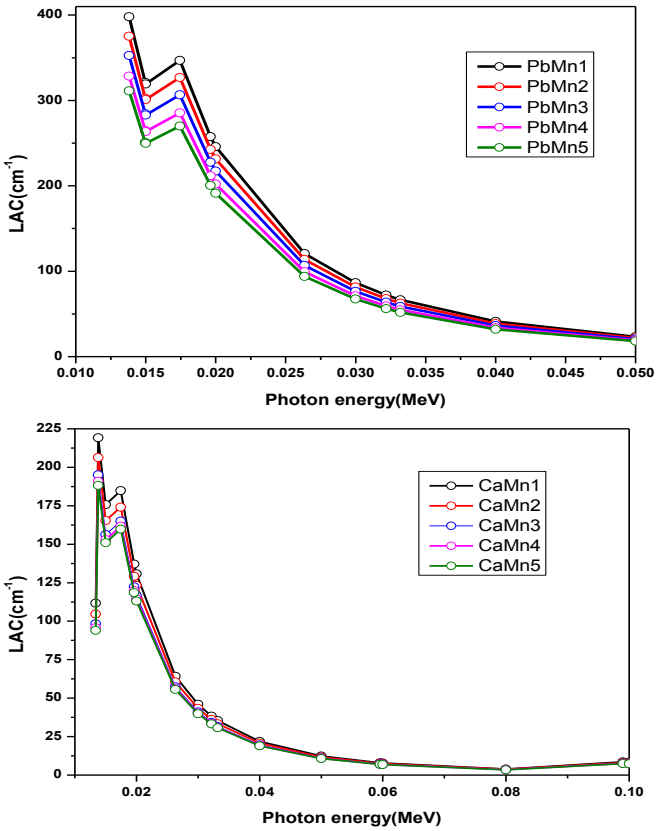

Fig. 3. LAC of PbMn and CaMn

3.5. Half-value layer (HVL)

The HVL curves shown in **Figure 4,** demonstrate that, especially in the low-energy (photoelectric) region, Pb–Bi–containing glasses need significantly less thickness (PbMn-1: 0.00164cm at 0.0138 MeV) than Ca–based glasses (CaMn-1:0.0062 cm at 0.0138 MeV) to attenuate photons. As photoelectric processes diminish and Compton scattering takes over, HVL rises quickly with photon energy to a wide maximum in the 2–6 MeV range [8]. At extremely high energies, it exhibits a modest fall because of growing pair-production contributions in high-Z elements.

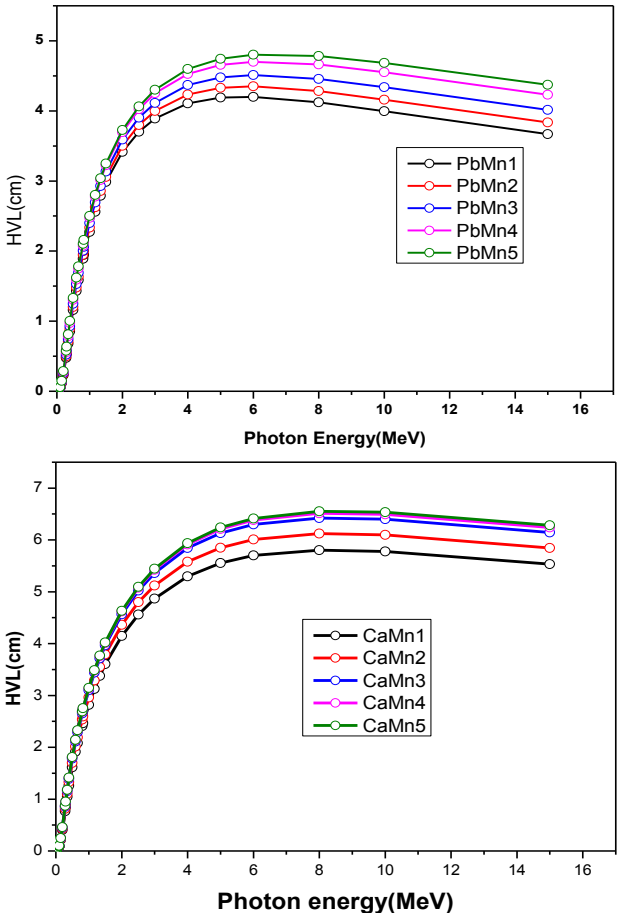

Fig. 4. HVL of PbMn and CaMn

3.6. Effective atomic number (Z_{eff})

The effective atomic number (Z_{eff}) of both Pb–Mn and Ca–Mn borate glasses significantly decline with photon energy, because the photoelectric effect predominates in the low-energy region (0.02–0.1 MeV) as shown in **Figure 5**. Due to the existence of high-Z PbF_2, Pb-based glasses show much higher Z_{eff} (up to ~77.99) than Ca-based glasses (~67.69). Z_{eff} becomes almost constant in the intermediate energy range (0.1–1 MeV), indicating Compton scattering's weak Z-dependence. The beginning of pair creation is correlated with a little rise in Z_{eff} above 1 MeV [9,10]. Variations in Al lead to slight variations among the compositions. In the case of PbMn glasses, Z_{eff} decreased, whereas in CaMn glasses, Z_{eff} increased with the gradual addition of Al_2O_3.

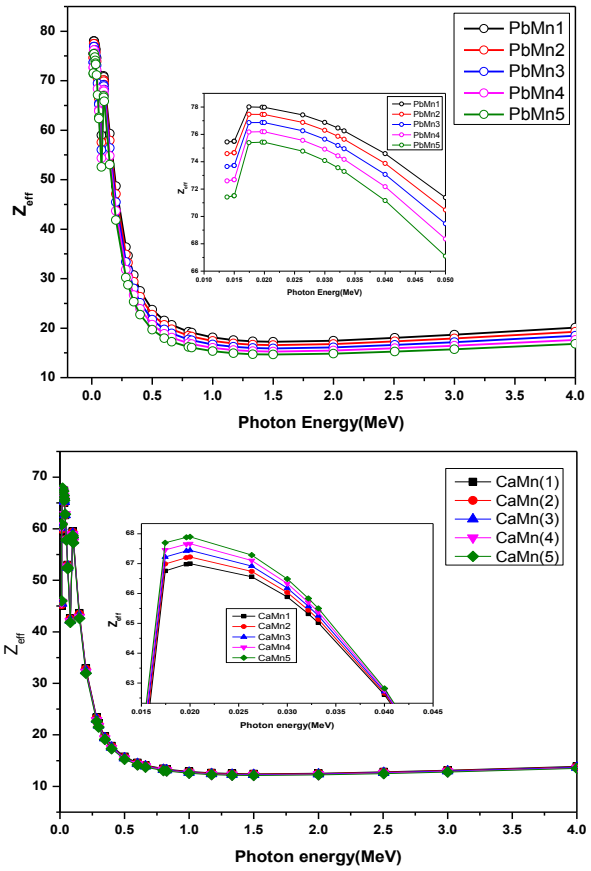

Fig. 5. Z_{eff} of PbMn and CaMn

3.7. Fast Neutron Removal Cross Section (Σ_r)

The fast neutron removal cross section (Σ_r), one of the neutrons' shielding characteristics, is a key measure of a material's capacity to attenuate fast neutrons and, consequently, determine if it is suitable for radiation shielding applications. This shows the probability of fast neutron attenuation per unit length of path through shielding substance [11,12]. Values of fast neutron removal cross section of PbMn and CaMn are given in **Table 3**. With an increase in Al_2O_3 concentration and a matching decrease in PbF_2, the rapid neutron removal cross section (σ_r) of PbMn glasses steadily rises from 0.1020 to 0.1053 cm^{-1}. This improvement is explained by the increased boron concentration, which promotes subsequent neutron absorption, and the enhanced elastic scattering efficiency of Al nuclei, which efficiently moderates fast neutrons. PbMn–S_5 has the greatest Σ_r value among the examined samples, suggesting that it is better suited for rapid neutron shielding applications. As the percentage of Al_2O_3 increases and the CaF_2 content declines, the rapid neutron removal cross section (Σ_r) of CaMn glasses falls from 0.1082 to 0.0987 cm^{-1}. The effective elastic scattering of fast neutrons by Ca and F nuclei is responsible for the high Σ_r value of CaMn–S_1. As CaF_2 gradually decreases, fewer effective scattering centres become available, which lowers the efficiency of neutron removal. These findings demonstrate that CaF_2 plays a major part in the CaMn glass system's rapid neutron attenuation.

Table 3. Fast neutron removal cross-section values of PbMn and CaMn Samples

Fast neutron removal cross section (cm^{-1})		
Sample	**PbMn**	**CaMn**
S_1	0.1020	0.1082
S_2	0.1024	0.1034
S_3	0.1028	0.1034
S_4	0.1029	0.0985
S_5	0.1053	0.0987

4 Conclusions

PbMn, CaMn glasses were examined for radiation shielding efficacy. Because high-Z PbF_2 was present, the Pb-based glasses consistently displayed greater MAC and LAC values, especially at low photon energy. As a consequence, their enhanced attenuation capability was confirmed by decreased HVL values. Ca-based glasses performed steadily in the mid-energy range but showed relatively less attenuation, as indicated by higher HVL values. These tendencies were further supported by Z_{eff} analysis: Ca-glasses showed reasonable Z_{eff} values with little variation among compositions, while Pb-containing glasses showed a very high Z_{eff} in the low-energy area with a sharp fall in the Compton region. These characteristics were very slightly affected by the modest compositional differences in MnO_2 and Al_2O_3, with PbMn1 and CaMn1 typically performing best because of their increased fluoride concentration. Overall, Pb–Mn glasses are more effective gamma-ray shielding materials, particularly for low and medium photon energies, according to the combined MAC, LAC, HVL, and Z_{eff} data, whereas Ca–Mn glasses provide moderate shielding performance with strong structural and compositional stability. CaMn glasses achieve higher fast neutron attenuation at optimised compositions than PbMn. PbMn glasses can be used for: Radiation medical facilities, nuclear facilities, and Windows with gamma-ray shielding. CaMn glasses could be the better option in terms of minimal toxicity, lower weight, and cost-effectiveness is essential.

References

1. Z. A. Alrowaili, Norah Alomayrah, H.H.Saleh, Chahkrit Sriwunkum, Amani Alalawi, M. S. Al-Buriahi. *Eur. Phys. J. Plus* 140:32 (2025) https://doi.org/10.1140/epjp/s13360-025-05968-z
2. Salim Barbhuiya, Bibhuti Bhusan Das, Paul Norman, Tanvir Qureshi. *Structural Concrete.*; 26:1809–1855 (2025) DOI:10.1002/suco.202400519
3. M.S. Al-Buriahi, Recep Kurtulus, Canel Eke, Sultan Alomairy, I.O. Olarinoye. Heliyon 10 e40249 (2024) . https://doi.org/10.1016/j.heliyon.2024.e40249
4. H. Ali . Alomari. *J. Taibah Univ. Sci.*, 18, 2328370, (2024) DOI:10.1080/16583655.2024.2328370
5. E. Şakar, Özgür Fırat Özpolat, B. Alim, M. I. Sayyed, M. Kurudirek, (2019). https://doi.org/10.1016/ j.radphyschem.2019.108496
6. A.M. Norah Alsaif, Hanan Al-Ghamdi, R. A. Elsad, A. M. Abdelghany, Shaaban M. Shaaba, Y. S. Rammah, and M.Islam Nabil, *Mater. Sci. Mater. Electron*. 35:534 (2024)
7. Nurdan Karpuz. J Radiat Res Appl Sc.*16* 100689. (2023) https://doi.org/10.1016/j.jrras.100689 (2023)

8. Serpil Emikönel, İskender Akkurt. *Int. J. Comput. Exp. Sci. Eng. 11 3461-3464. (2025) DOI: 10.22399/ijcesen.2157*
9. M.S. Al-Buriahi, Z.A. Alrowaili, Sultan J. Alsufyani, Amani Alalawi, I.O. Olarinoye, Chahkrit Sriwunkum, Norah Salem Alsaiari.*J Radiat Res Appl Sc* 17 101153. (2024) https://doi.org/10.1016/j.jrras.2024.101153
10. K.A. Naseer, *Nexus of Future Materials* 2 177-181 (2025) https://doi.org/10.70128/593188
11. O.I. Sallam, A.M. Madbouly, N.A. Elalaily, F.M. Ezz-Eldin. *J. Alloys Compd. (2020). DOI: https://doi.org/10.1016/j.jallcom.2020.156056.*
12. F. Duru, D. Hughes, M.M. Christiansen, T. Caplice, H. Funk, R.S. Welch, M. Rusch, S. Simko, N.J. Keninger, J.K. Nimmagadda, J. Instrum.*, 19, (2024*).DOI 10.1088/1748-0221/19/09/P09011